Baroclinic Instability in High Latitudes Induced by Polar Vortex: A Connection to the Arctic Oscillation

H. L. TANAKA

Institute of Geoscience, University of Tsukuba, Tsukuba, Japan, and Frontier Research System for Global Change, International Arctic Research Center, University of Alaska, Fairbanks, Alaska

HIROKI TOKINAGA

Graduate School of Environmental Earth Science, Hokkaido University, Sapporo, Japan

(Manuscript received 9 June 2000, in final form 4 June 2001)

ABSTRACT

In this study, baroclinic instability of the northern winter atmosphere is investigated in the context of the dynamical interpretation of the Arctic oscillation. The unstable solutions, obtained by a method of 3D normal mode expansion, are compared for observed zonal basic states with strong and weak polar vortices in reference to the Arctic oscillation index.

As a result of the eigenvalue problem of the linear stability analysis, a characteristic unstable solution is obtained that dominates in high latitudes when the polar vortex is strong. The mode is called a monopole Charney mode M_1, which is similar to an ordinary Charney mode M_C in midlatitudes. In order to understand the origin of the M_1 mode, a hypothetical zonal basic state that has only the polar jet with no subtropical jet is analyzed. It is found that the M_1 mode in high latitudes is excited by the baroclinicity associated with the polar vortex. The M_1 mode in high latitudes is dynamically the same Charney mode as M_C but is excited by the baroclinicity of the polar jet instead of the subtropical jet.

As the M_C mode intensifies the subtropical jet by the eddy momentum transfer, the M_1 mode transfers eddy momentum to high latitudes to intensify the polar jet. Since M_1 mode appears during the strong polar jet and feeds the westerly momentum to the polar jet, there is a positive feedback between the M_1 mode and the polar vortex. This positive feedback would produce a persistent strong polar jet, which may in tern result in the occurrence of the annular mode of the Arctic oscillation.

1. Introduction

Arctic oscillation (AO) advocated by Thompson and Wallace (1998) has attracted more attention in recent years. The AO is a north–south seesaw of the atmospheric mass between the arctic region poleward of 60°N and a surrounding zonal ring in midlatitudes. It is defined as a primary mode of an empirical orthogonal function (EOF) for the sea level pressure field in the Northern Hemisphere (NH).

The spatial pattern of the AO is characterized by its zonally symmetric or ''annular'' structure of the sea level pressure, centered at the Arctic. In this regard, a terminology of ''annular mode'' may be much suitable. Such an annular mode was documented early in the 1920s in the literature by Exner (1925) using a correlation map of the sea level pressure in the Arctic and the surrounding lower latitudes. The areas of positive and negative correlations are separated by a ring of the zero correlation line appearing at the latitudes of 50°–60°N. The concept of such a northern oscillation in the sea level pressure was originally a counterpart of the Southern Oscillation due to the Walker circulation along the equatorial Pacific.

The north–south seesaw in the sea level pressure relates to the meridional gradient of the geopotential, whereby it links to the wintertime polar jet along the Arctic circle. According to the observational analysis, the AO has an equivalent barotropic structure from the surface to the lower stratosphere in that the positive or negative geopotential anomaly occurs consistently from the troposphere to the stratosphere (Kodera et al. 1996; Kitoh et al. 1996; Thompson and Wallace 1998)

Although not exactly relevant, the classic concept of a zonal index introduced by Namias (1950) should have a close connection to the present AO. Strong westerly jet with high baroclinicity (high index) excites baroclinic disturbances in the midlatitudes in order to eliminate the baroclinicity by the meridional mixing of mass and energy. The resulting low baroclinicity (low index) with weak westerly soon recovers to the high index by

Corresponding author address: Dr. H. L. Tanaka, Institute of Geoscience, University of Tsukuba, Tsukuba 305-8571, Japan.
E-mail: tanaka@atm.geo.tsukuba.ac.jp

the meridional differential heating assisted by the heat transport due to Hadley circulation. The AO is associated with the intensity of the polar jet, only the difference between the AO and the index cycle seems to be the latitude where the oscillation occurs.

The AO bears a superficial resemblance to the leading mode of low-frequency variability in the Southern Hemisphere (SH), which is now referred to as a southern annular mode (SAM). The structure and dynamics of the SAM have been extensively documented (e.g., Shiotani 1990). Vacillation of the annular mode in the SH is caused by the oscillatory feedback of the westerly momentum transfer by the synoptic disturbances. The similarity between the NH and SH may be the reflection of the common dynamical processes. Yet the understanding for the dynamics of the AO is still an open question. Although the spatial structures of those annular modes are similar, the time spectrum of the AO is quite red with no preferred periodicity.

Recently, Yamazaki and Shinya (1999) conducted seasonal and perpetual February runs to simulate the AO using only the internal dynamics of the atmospheric general circulation model developed by the Center for Climate System Research, National Institute for Environmental Studies. They confirmed that the AO is an intrinsic internal mode of the atmosphere. Their results indicate that the wave–mean flow interactions are responsible for the phase transition between the positive and negative polarity of the AO. They also find that the planetary-scale wavenumbers 2 and 3 play the largest contribution among the zonal eddies, while the synoptic-scale waves contribute destructively. The results suggest that the baroclinic instability in the planetary-scale wavenumbers 2 and 3 plays an important role. It may be interesting to study the different roles of baroclinic instability in synoptic and planetary waves in the context of the dynamical understanding of the AO.

The purpose of this study is to analyze the baroclinic instability in synoptic and planetary waves given specific zonal mean basic states with strong and weak polar vortices. Baroclinic instability is, in general, induced by the baroclinicity associated with the subtropical jet. We are interested more in the baroclinicity in high latitudes associated with the polar vortex in this study. Therefore, we first define the overall intensity of the polar vortex in reference to the AO index. Then, the baroclinic instability is analyzed both for the high and low AO indices. The results of the dominant unstable modes are compared for their growth rate, phase speed, and the structure. The expected feedback to the zonal mean basic states of the strong and weak polar vortices is discussed.

In this study, a 3D spectral primitive equation model in terms of the 3D normal mode expansion developed by Tanaka and Kung (1989) is used in order to solve the linear baroclinic instability for general zonal mean basic states on a sphere. The zonal mean basic states, which represent both the subtropical jet and polar jet, are constructed from wintertime monthly and seasonal mean observational data using the National Centers for Environmental Prediction–National Center for Atmospheric Research (NCEP–NCAR) reanalysis (Kalnay et al. 1996). Although the model is based on the primitive equations on a sphere, we can filter out the redundant unstable gravity modes by virtue of the normal mode expansion technique.

In section 2 the data and governing equations are described for the linear baroclinic instability problem. In section 3 an index for the intensity of the polar vortex is introduced in reference to the AO index. The results of the stability analyses are presented for a weak polar vortex in section 4 and for a strong polar vortex in section 5. In section 6 the identification and dynamical interpretation are attempted for the most unstable mode in high latitudes. Finally, the relevance of the conclusions in this study to the dynamical interpretation of the AO is discussed in section 7.

2. Data and method

a. Data for the zonal mean basic state

The data used in this study are twice daily (0000 and 1200 UTC) reanalysis provided by NCEP and NCAR for 1950–98 (see Kalnay et al. 1996). The data contain horizontal winds $V = (u, v)$, vertical p velocity ω, temperature T, and geopotential ϕ, defined at every 2.5° latitude × 2.5° longitude grid point over 17 mandatory vertical levels from 1000 to 10 hPa. Zonal mean data for those variables are averaged for every month. Wintertime mean data are also edited by averaging the monthly mean data for December to February (DJF).

b. Governing equations

The detail of the model description is provided by Tanaka (1998), so a brief description is presented here. A system of primitive equations with a spherical coordinate of longitude λ, latitude θ, pressure p, and time t may be reduced to three prognostic equations of horizontal motions and thermodynamics for three dependent variables of $\mathbf{U} = (u, v, \phi')^{\mathrm{T}}$. Here, u and v are the zonal and meridional components of the horizontal velocity V, and the superscript T denotes a transpose. The variable ϕ' is a departure of the local isobaric geopotential from the reference state geopotential ϕ_0, which is related through the hydrostatic equation to the reference state temperature T_0. Using a matrix notation, these primitive equations may be written as

$$\mathbf{M}\frac{\partial \mathbf{U}}{\partial t} + \mathbf{L}\mathbf{U} = \mathbf{N} + \mathbf{F}, \tag{1}$$

where the left-hand side of (1) represents linear terms with matrix operators $\mathbf{M}$ and $\mathbf{L}$ and the dependent variable vector $\mathbf{U}$. The matrix $\mathbf{M}$ is referred to as a mass matrix, which is nonsingular and positive definite under

a proper boundary conditions. The right-hand side represents a nonlinear term vector **N** and a diabatic term vector **F**, which includes the zonal F_u and meridional F_v components of frictional forces and a diabatic heating rate Q.

In order to obtain a system of spectral primitive equations, we expand the vectors **U** and **F** in 3D normal mode functions in a resting atmosphere, $\Pi_{nlm}(\lambda, \theta, p)$:

$$U(\lambda, \theta, p, t) = \sum_{nlm} w_{nlm}(t)\mathbf{X}_m\Pi_{nlm}(\lambda, \theta, p), \quad (2)$$

$$F(\lambda, \theta, p, t) = \sum_{nlm} f_{nlm}(t)\mathbf{Y}_m\Pi_{nlm}(\lambda, \theta, p). \quad (3)$$

Here, the dimensionless expansion coefficients $w_{nlm}(t)$ and $f_{nlm}(t)$ are the functions of time alone. The subscripts represent zonal wavenumbers n, meridional indices l, and vertical indices m. They are truncated at N, L, and M, respectively. The scaling matrices $\mathbf{X}_m$ and $\mathbf{Y}_m$ are defined at each vertical index. The expansion basis of the 3D normal mode functions in a resting atmosphere $\Pi_{nlm}(\lambda, \theta, p)$ is obtained as eigensolutions of a homogeneous partial differential equation, putting zero for the right-hand side of (1). The 3D normal mode functions are given by a tensor product of vertical structure functions $G_m(p)$ and Hough harmonics $H_{nlm}(\lambda, \theta)$ associated with the linear operators **M** and **L**, respectively. It is known that they form a complete set and satisfy an orthonormality condition under a proper inner product.

According to the Galerkin method (see Kasahara 1984), the same boundary conditions as the normal modes are imposed to the model atmosphere since we have assumed that the atmospheric state variables are expandable with the 3D normal mode functions. The lower boundary condition is therefore derived from the condition of a vanishing wind vector that consists of horizontal u, v, and vertical $w = dz/dt$ wind speeds:

$$(u, v, w) = 0, \quad \text{at } p = p_s. \quad (4)$$

The upper boundary condition is given by statements that bound total kinetic and available potential energies:

$$\int_0^{p_s} K + A\, dp < \infty. \quad (5)$$

By expanding those variables in 3D normal model functions, we obtain a system of 3D spectral primitive equations in terms of the spectral expansion coefficients:

$$\frac{dw_i}{d\tau} + i\sigma_i w_i = -i \sum_{jk} r_{ijk} w_j w_k + f_i, \qquad i = 1, 2, 3, \ldots \quad (6)$$

where τ is a dimensionless time scaled by $(2\Omega)^{-1}$, σ_i is the eigenfrequency of the Laplace's tidal equation, and r_{ijk} is the interaction coefficients for nonlinear wave–wave interactions. The triple subscripts are shortened for simplicity as $w_{nlm} = w_i$. There should be no confusion in the use of i for a subscript even though it is used for the imaginary unit.

c. Eigenvalue problem for linear instability analysis

Next, the nonlinear spectral equation (6) is linearized for a prescribed zonal basic state in order to study the barotropic–baroclinic instability. A perturbation method is introduced using notations $\overline{w}_i$ for a time-independent zonal basic state and w' for small perturbations superimposed on the basic states (the same symbols with the original variables are used for convenience). The equation for the first-order term of perturbations for each zonal wavenumber becomes

$$\frac{dw_i}{d\tau} + i\sigma_i w_i = -i \sum_{j=1}^{K} \left[\sum_{k=1}^{K} (r_{ijk} + r_{ikj})\overline{w}_k \right] w_j, \qquad i = 1, 2, 3, \ldots, K, \quad (7)$$

where the index k is used for the basic state and i and j for the perturbations. An inviscid and adiabatic eddy is examined here, disregarding the forcing. For a zonal basic state ($\overline{w}_k \neq 0$ if $n = 0$), we can rewrite the equation above in terms of a matrix form for each $n \geq 0$:

$$\frac{d}{d\tau}W_n + i\mathbf{D}_n W_n = -i\mathbf{B}_n W_n, \qquad n = 1, 2, \ldots, N, \quad (8)$$

where $W_n = (w_1, \ldots w_i, \ldots w_K)^{\mathrm{T}}$, $\mathbf{D}_n = \mathrm{diag}(\sigma_1, \ldots \sigma_i, \ldots \sigma_K)$, and $K = (L + 1)(M + 1)$. The (i, j) entries of the matrices $\mathbf{B}_n$, namely b_{ij}, are evaluated by the expansion coefficients of the basic state $\overline{w}_k$ as seen on the right-hand side of (7). The zonal–wave interaction $\mathbf{B}_n$ vanishes for a basic state at rest ($\overline{w}_k = 0$), thus (8) satisfies the normal mode relation for Laplace's classic tidal theory.

Because (8) is linear, we can assume the solution of W_n as

$$W_n(\tau) = \xi \exp(-i\nu\tau). \quad (9)$$

The initial value problem (8) is then reduced to an eigenvalue problem for a real matrix to obtain eigenvectors ξ and eigenvalues ν as

$$\nu\xi = (\mathbf{D}_n + \mathbf{B}_n)\xi. \quad (10)$$

Those eigenpairs ν and ξ are evaluated by the standard matrix eigenvalue solver.

The applicability of the present spectral method for a linear instability problem is demonstrated by Kasahara and Tanaka (1989). The result of the growth rate, phase speed, and modal structure are compared with previous studies in the quasigeostrophic framework. The dynamical interpretation for the imposed boundary condition is discussed in detail. The growth rates and the structure of the unstable modes are first discussed in the framework of primitive equations by Tanaka and Kung (1989) and Tanaka and Sun (1990) using a basic state of month-

ly mean First Global Atmospheric Research Program Global Experiment data for January 1979. A few modes indicate nonnegligible growth rates, but most of eigenmodes are close to be neutral. The so-called Charney mode dominates in the synoptic scale. The growth rate of the most unstable Charney mode is about 0.47 day^{-1} at the zonal wavenumber 7, which corresponds to an *e*-folding time of about 2 days.

Since the unstable modes are solved over the sphere with an open boundary at the top of the atmosphere, a Burger mode (Burger 1958), which has a nodal structure in the vertical, may be analyzed. The first Burger mode with one node is called Green mode (Green 1960). Likewise, meridional dipole mode may be analyzed as a variation of the higher-order Charney mode with one nodal structure in the meridional, as discussed by Tanaka and Kung (1989). It is found that the most unstable modes in planetary waves are not the ordinary Charney mode but a dipole Charney mode, which has a meridional dipole structure in the geopotential amplitude. According to Tanaka and Kung (1989), a unique variation of Charney mode with a monopole structure was analyzed in the planetary waves. The mode was referred to as monopole Charney mode M_1. Its structure is quite similar to the standard Charney mode, but it appears in high latitudes. It is certainly not the variation of the higher-order Charney mode such as the Green mode or dipole Charney mode. In this study, however, the M_1 mode appears to be the key unstable mode in relation to the AO as will be discussed later.

3. Arctic oscillation index and polar vortex index

The AO is defined in Thompson and Wallace (1998) by the EOF-1 of the sea level pressure in the Northern Hemisphere during the winter (November–April mean). An axisymmetric pressure pattern with opposite sign in low and high latitudes may be the main characteristics of AO. In this regard, a terminology of annular mode may be quite suitable. The zero crossing of the pressure contour is seen around 60°N. The close looking at the AO pattern indicates two minor peaks in the pressure pattern over North Pacific and North Atlantic. Some consider that those two minor peaks over oceans are also the important ingredient of AO in relation to North Atlantic oscillation and Pacific–North America patterns (Wallace and Gutzler 1981).

It may be our consensus now that AO has a barotropic structure in that the axisymmetric pressure pattern of the EOF-1 is detected at the whole vertical levels in the troposphere as well as in the lower stratosphere. For this reason, we examined the barotropic component of the geopotential height in this study in the framework of the 3D normal model expansion and compared the pattern with that for the sea level pressure. Here, the barotropic component of the geopotential height Z_0 is defined by the vertical integral of the geopotential height deviation Z' from its global mean:

$$Z_0 = \frac{1}{p_s}\int_0^{p_s} Z' G_0 \, dp, \tag{11}$$

where p_s is the surface pressure of the reference state and G_0 is the vertical structure functions for the barotropic component (see Tanaka 1998). The barotropic component represents the overall features of the general circulation of the atmosphere.

Figure 1 illustrates the EOF-1 of the sea level pressure and the barotropic component of the geopotential height during wintertime mean (November to April) evaluated from the NCEP–NCAR reanalysis during 1950–98. The original time series data are detrended before the EOF analysis. As expected, the EOF-1 for the barotropic component of the geopotential height is almost identical to that analyzed for the sea level pressure (see Thompson and Wallace 1998). Closed contours with negative sign are seen over the circumpolar vortex. Two centers of action of positive values over North Pacific and North Atlantic are superimposed on the zonally symmetric positive area surrounding the polar vortex. The intensity of the positive area over the North Pacific is stronger than that over the North Atlantic for the barotropic component of the geopotential height. Since the AO pattern for the sea level pressure and/or 1000-hPa geopotential height shows comparable intensity for the Pacific and Atlantic centers of action, the present result suggests that the Pacific center is more barotropic and the Atlantic center is more baroclinic in their anomaly fields.

Figure 2 compares the time series of EOF-1 scores associated with the sea level pressure and the barotropic component of the geopotential fields, respectively. The time series for the sea level pressure (solid line) is defined as an Arctic oscillation index (AOI). The positive value AO(+) indicates negative pressure anomaly over the Arctic, whereas the negative value AO(−) indicates positive pressure anomaly there. The Beaufort high is weakened when the AOI is positive and is intensified when the AOI is negative there. The notable time variation of the AOI in Fig. 2 is the two abrupt changes that occurred in 1976/77 and in 1988/89. The large positive AOI shifts to negative AOI after 1976/77, then it shifts to large positive AOI after 1988/89. The index suggests that the Beaufort high was strong during the decade from 1976/77 to 1988/89, then it was weak after 1988/89. It is shown by Walsh et al. (1996) that the anticyclonic circulation associated with the Beaufort high is reversed to cyclonic circulation after 1988/89. The AOI is returning from positive to negative during 1990s, suggesting that the Beaufort high is returning to its full strength by the year 2000.

The time series for the barotropic component of geopotential height (dashed line) captures the essential part of the AOI; the major fingerprint of the two abrupt changes in 1976/77 and 1988/89 in the AOI is detected clearly. Since the time series describes the variation of the whole vertical column of the pressure anomaly field, the positive value implies stronger polar vortex with a

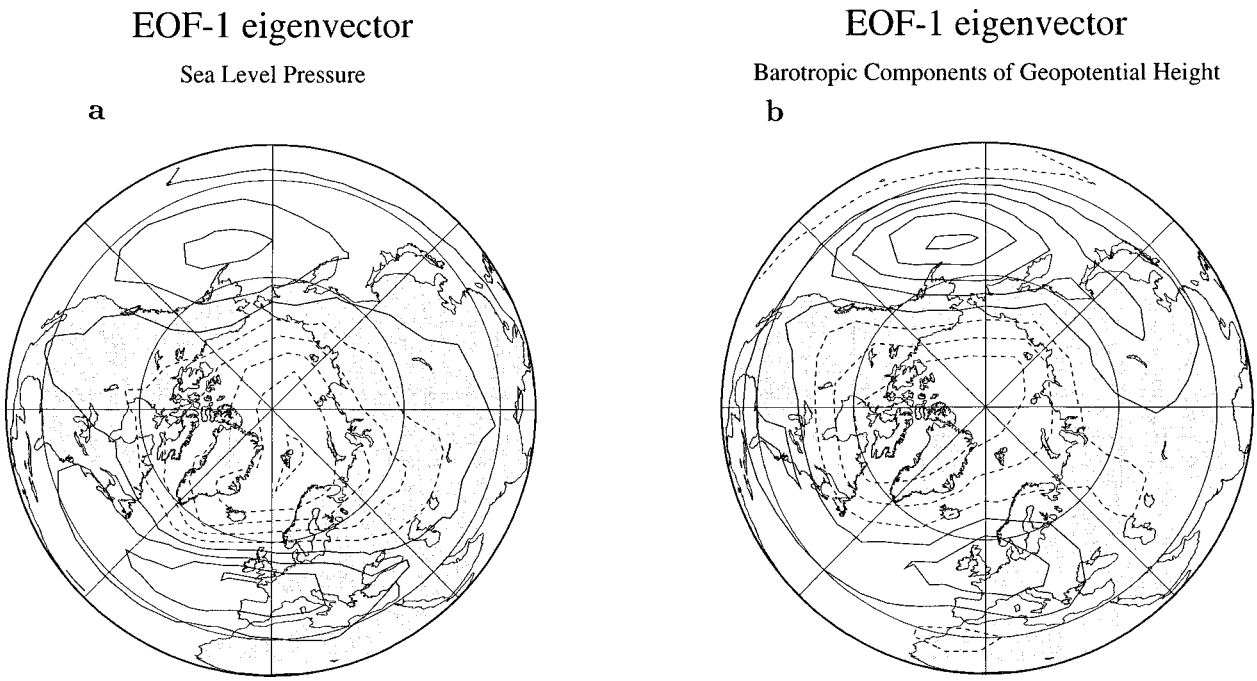

FIG. 1. The AO pattern obtained by (a) the EOF-1 of the sea level pressure and (b) the barotropic component of geopotential height in the NH using the NCEP–NCAR reanalysis for 1950–98.

sharp pressure gradient near 60°N. Conversely, the negative value implies weaker polar vortex with weaker pressure gradient there. In this regard, we may define the time series (dashed line) as an index that measures the mean polar vortex intensity (PVI). We should note here that the PVI represents the intensity of the vertically integrated polar vortex rather than that in the stratosphere as is originally defined. Although the states of strong polar vortex PV(+) and weak polar voretx PV(−) do not correspond perfectly to the AO(+) and AO(−), respectively, we consider those indicies of AOI and PVI represent dynamically consistent states with each other.

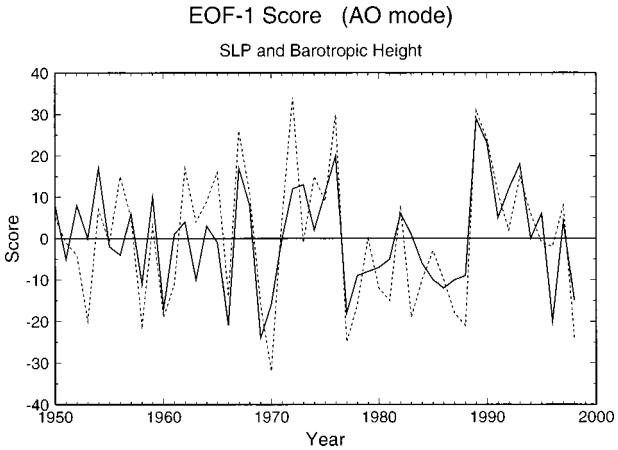

FIG. 2. Time series of the score of the EOF-1 during 1950–98 for the sea level pressure (solid line) and the barotropic component of geopotential height (dashed line).

The PVI shows that the strong mean polar vortex is weakened abruptly after 1976/77, and it returns to strong phase abruptly after 1988/89. It is consistent with AOI in that the intensified mean polar vortex destroyed the surface Beaufort high so that the anticyclonic circulation reversed to cyclonic circulation. Proshutinsky and Johnson (1997) showed that the reversing atmospheric circulation over the Arctic Ocean changes the rotation of sea ice move. The impact of the AO phase shift for the decadal variability of the arctic climate system is considerable. The PVI returns from positive to negative in the late 1990s.

The AOI represents the variation of total mass of the atmospheric vertical column because the index is derived from the surface pressure. In comparison, the PVI represents the vertically integrated pressure anomaly that directly connects with the wind anomaly through the geostrophic wind relation. In the following sections, the characteristics of baroclinic instability are compared for the strong polar vortex winter and the weak polar vortex winter based on the PVI in Fig. 2. We analyzed six typical winters: 1988/89 and 1992/93 for the strong polar vortex, and 1976/77, 1984/85, 1986/87, 1997/98 for the weak polar vortex. Among those, we present the cases of 1997/98 and 1986/87 representing the weak polar vortex in section 4, and the cases of 1988/89 and 1992/93 representing the strong polar vortex in section 5.

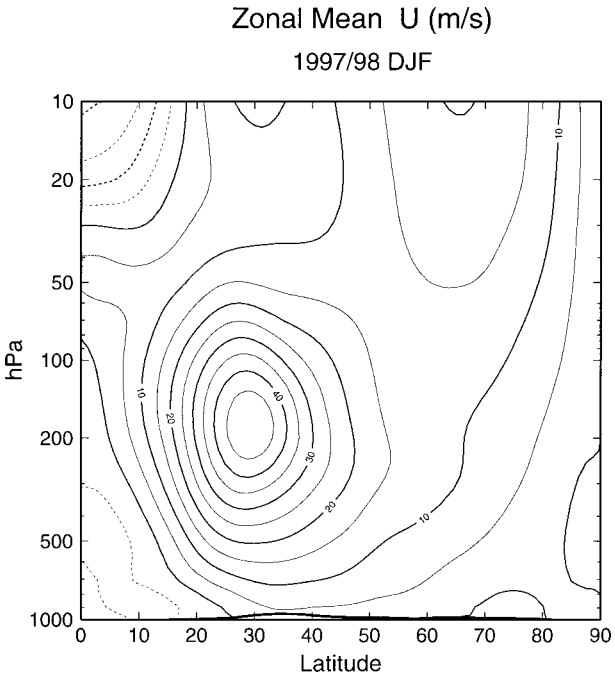

FIG. 3. Meridional-height section of zonal mean zonal wind (m s^{-1}) for DJF in 1997/98 (weak polar vortex) in the NH.

4. Results for weak polar vortex

a. A case for 1997/98

The winter of 1997/98 shows a typical weak polar vortex as presented in Fig. 3 for the DJF mean. The meridional-height section of zonal mean zonal wind indicates the wind speed of at most 20 m s^{-1} of polar night jet at 10-hPa level, while the subtropical jet over 30°N is 45 m s^{-1}. The former winter of 1996/97 is known to have shown a strong and persistent circumpolar vortex, which causes a prominent Arctic ozone loss in March of 1997 (Bell and Halpert 1998). It was anticipated that the Arctic ozone loss might expand, as in the Antarctic. However, the decadal time series of the PVI in 1990s clearly suggests that the mean polar vortex is weakened gradually in 1990s after 1988/89. Contrasted with the winter of 1996/97, the following winter of 1997/98 experienced a sequence of stratospheric sudden warming, which resulted in a very weak polar vortex, as in Fig. 3. The anticipated expansion of the ozone loss was absent in this winter and also in the following winters.

Figure 4 illustrates the growth rates (day^{-1}) and phase speeds (° day^{-1}) of the unstable modes computed for the zonal mean basic state of the weak polar vortex in 1997/98. The most unstable mode at the zonal wavenumber $n = 7$ may be identified as Charney mode, which appears for $n = 3$ to 12 (see Charney 1947; Simmons and Hoskins 1976; Tanaka and Kung 1989). The growth rate is approximately 0.4 day^{-1} with its *e*-folding time of 2.5 days. It moves eastward with its

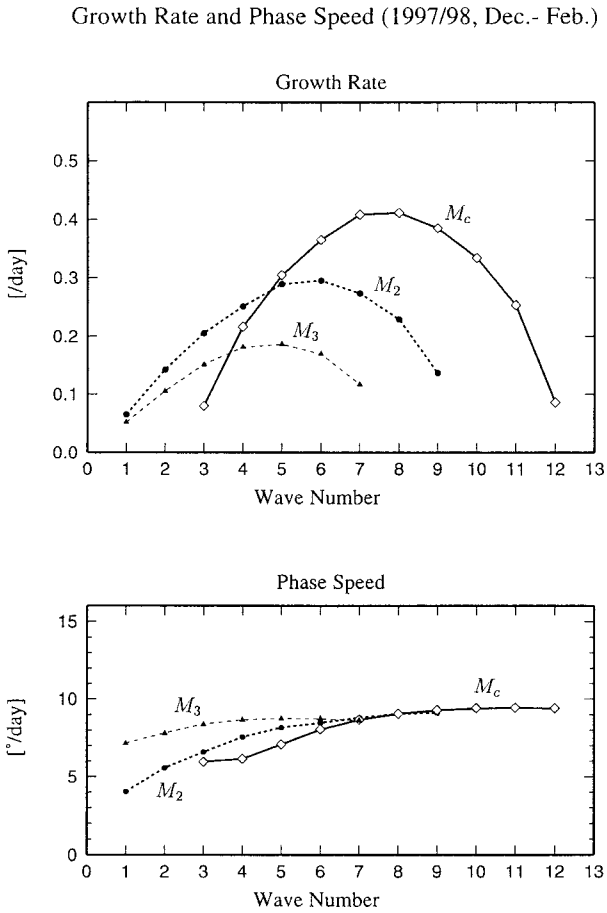

FIG. 4. Growth rates (day^{-1}) and phase speeds (° day^{-1}) of the unstable modes for the zonal mean basic state of the weak polar vortex in 1997/98. The unstable modes are labeled M_C for ordinary Charney modes, M_2 for dipole Charney modes, and M_3 for tripole Charney modes.

phase speed of approximately 8° day^{-1} advected by the mean westerly. The most unstable mode is replaced by another different mode for the zonal wavenumbers $n =$ 1 to 4, which clearly has different modal structure. With the use of the 3D normal mode expansion technique, the baroclinically unstable modes in planetary waves are examined comprehensively. According to Tanaka and Kung (1989), those unstable modes are labeled as shallow Charney modes M_C, dipole Charney modes M_2, and tripole Charney modes M_3, observing their structures as below.

The meridional-height structures of the geopotential amplitude (in arbitrary unit) and phase (in longitude of ridges) are plotted in Fig. 5 for the ordinary Charney modes M_C at $n = 6$ and 8, dipole Charney modes M_2 at $n = 3$ and 4, and tripole Charney modes M_3 at $n =$ 3 and 4, respectively. The ordinary Charney modes M_C at $n = 6$ indicate the amplitude maximum at the upper troposphere near 50°N. The phase tilts westward with respect to height, transporting the eddy heat energy to the north. The amplitude peak moves down to the sur-

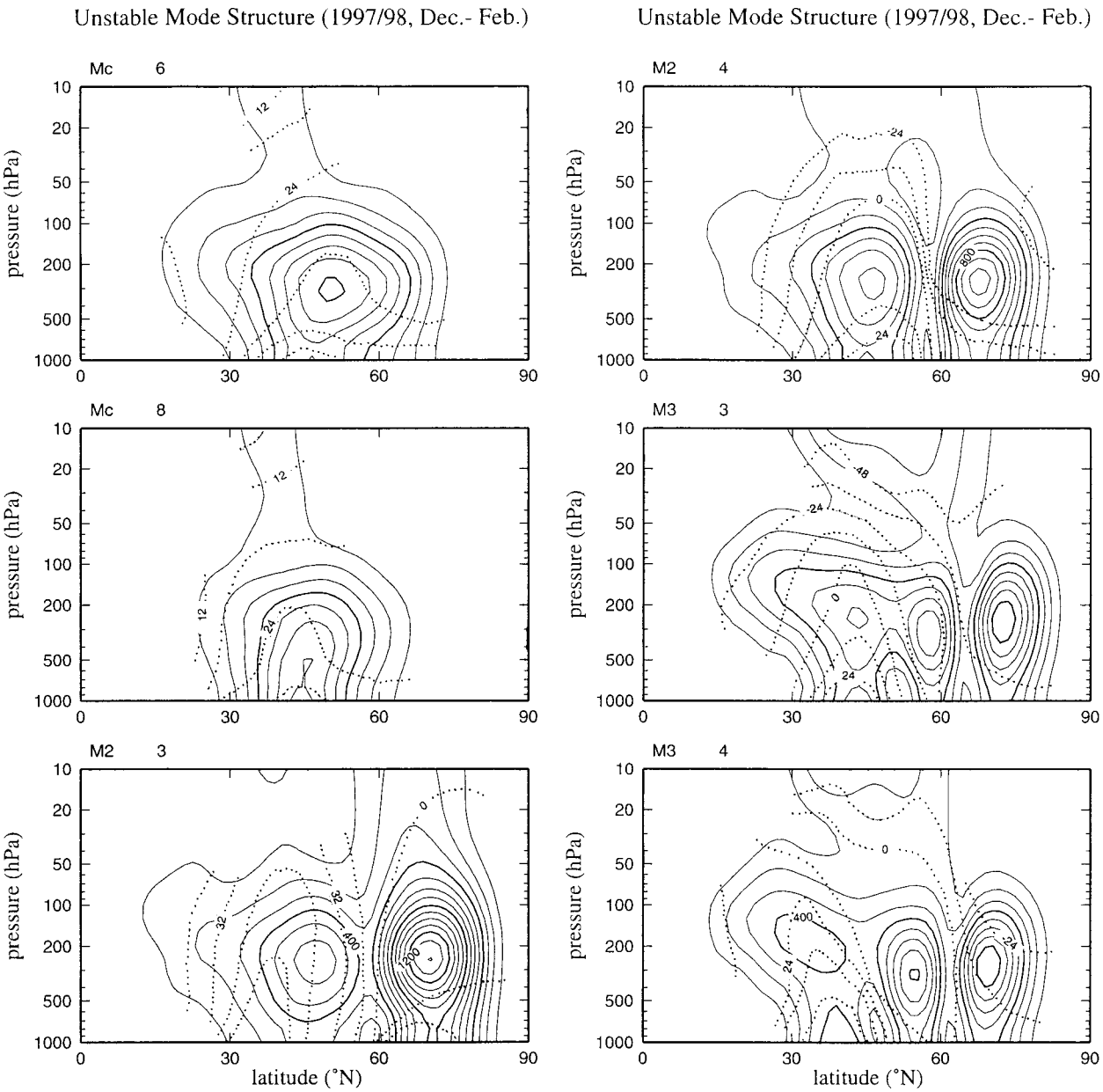

FIG. 5. Meridional-height section of the geopotential amplitude (in arbitrary unit) and phase (in longitude of ridges) for M_C at zonal wavenumbers $n = 6$ and 8, M_2 at $n = 3$ and 4, and M_3 at $n = 3$ and 4 in Fig. 4.

face for $n = 8$. The phase structure indicates that eddy momentum flux is northward at 30°N and southward at 60°N, so it converges at 45°N. The M_C mode is clearly excited by the baroclinicity associated with the subtropical jet near 30°N. The eddy tends to intensify the subtropical jet especially at the northern flank of the jet. Obviously, there is a certain kind of positive feedback between the subtropical jet and the baroclinic instability of the M_C mode. A detailed analysis in terms of the normal mode energetics (see Tanaka and Kung 1988) suggests that the energy source for those baroclinic eddies is available potential energy associated with the baroclinicity of the subtropical jet. Kinetic energy of the excited eddies is then transformed to the lower part of the subtropical jet, reducing the vertical shear (baroclinicity) of the jet. The kinetic energy accumulated near the surface is ultimately dissipated by the surface friction. Those structures and the nature of the eddies are consistent with previous studies (e.g., Simmons and Hoskins 1976; Tanaka and Kung 1989).

The dipole Charney mode M_2 indicates two amplitude peaks in the meridional section. The southern peak indicates westward phase tilt with respect to height as in M_C, while the northern peak indicates more barotropic

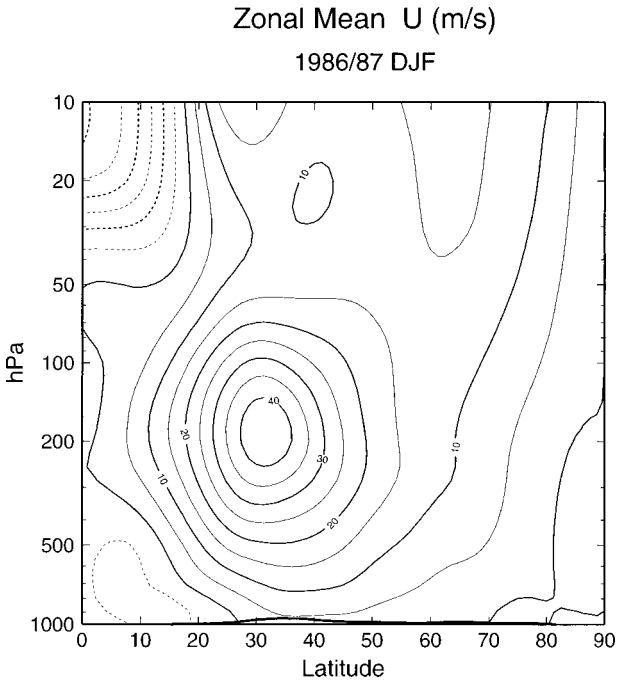

FIG. 6. As in Fig. 3 but for DJF in 1986/87 (another case of the weak polar vortex).

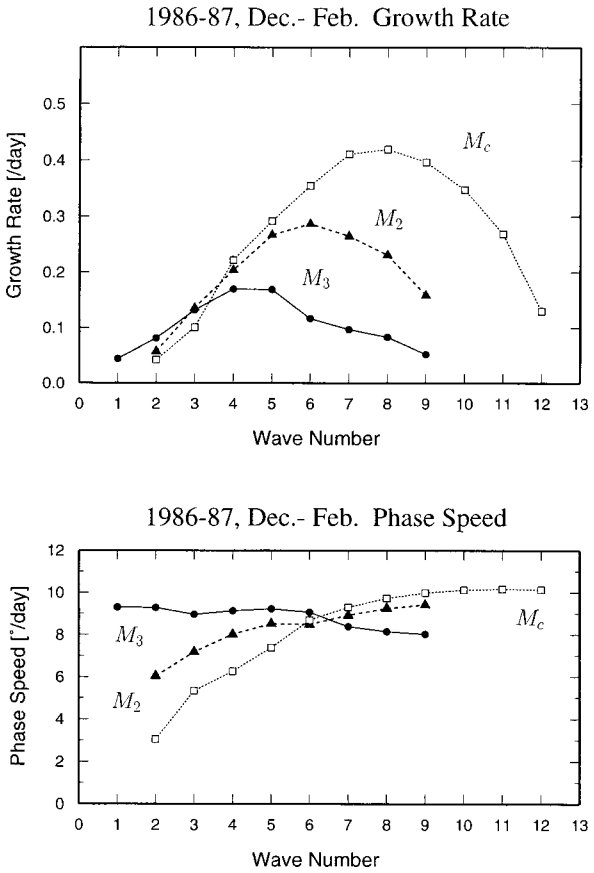

FIG. 7. As in Fig. 4 but for the weak polar vortex of 1986/87 in Fig. 6.

structure. The locations of ridges at the southern and northern amplitude peaks are out of phase, describing a blocking-like high–low vortex pair. The mode may be important to excite the blocking system with a meridional dipole structure as suggested by Tanaka and Kung (1989). In this study, we analyzed a tripole Charney mode M_3 that has three amplitude peaks in the meridional section. The existence of M_3 was predicted in our former studies, but the growth rate was too small to identify the mode. It appears in this study as the second most unstable mode in planetary waves for the weak polar vortex.

b. A case for 1986/87

The winter of 1986/87 is also the year of a typical weak polar vortex as presented in Fig. 6 for the DJF mean. The meridional-height section of zonal mean zonal wind indicates that the wind speed of polar night jet is at most 15 m s^{-1} at 10-hPa level while the subtropical jet over 30°N is 40 m s^{-1}. The wind distribution is quite similar to that of 1997/98 and is characterized by the absence of the polar night jet.

Figure 7 illustrates the growth rates (day^{-1}) and phase speeds (° day^{-1}) of the unstable modes analyzed for the weak polar vortex in 1986/87. The most unstable Charney mode M_C appears for $n = 2$ to 12. The growth rate is approximately 0.4 day^{-1} with its *e*-folding time of 2.5 days at the zonal wavenumber $n = 8$. It moves eastward with its phase speed of approximately 9° day^{-1} advected by the mean westerly. The second unstable mode is identified as dipole Charney mode M_2 from its meridional dipole structure. Likewise, the third unstable mode is identified as tripole Charney mode M_3. For planetary waves of $n = 1$ to 4, those three unstable modes of M_C, M_2, and M_3 have almost the same growth rate. In such an occasion, a traditional approach of computing the most unstable mode by time integration method (e.g., Hartmann 1979) would fail to converge since the iteration cannot separate the unstable solutions with nearly same growth rates.

5. Results for strong polar vortex

a. A case for 1988/89

We now compare the unstable modes for the zonal basic state with the strong polar vortex in 1988/89. Figure 8 illustrates the meridional-height section of zonal mean zonal wind (m s^{-1}) as in Fig. 3, but for DJF in 1988/89 with the strong polar vortex in the Northern Hemisphere. There is a strong polar night jet over 65°N in the stratosphere. The maximum wind speed in the figure is 40 m s^{-1} at 10-hPa level. The peak line in the wind speed is connected to the subtropical jet at the tropopause level over 30°N. The maximum wind speed

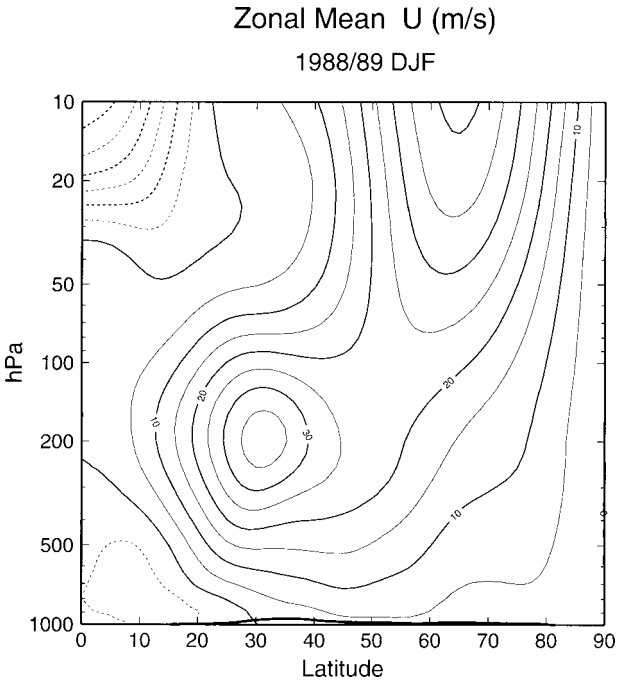

FIG. 8. Meridional-height section of zonal mean zonal wind (m s^{-1}) as in Fig. 3, but for DJF in 1988/89 (strong polar vortex) in the NH.

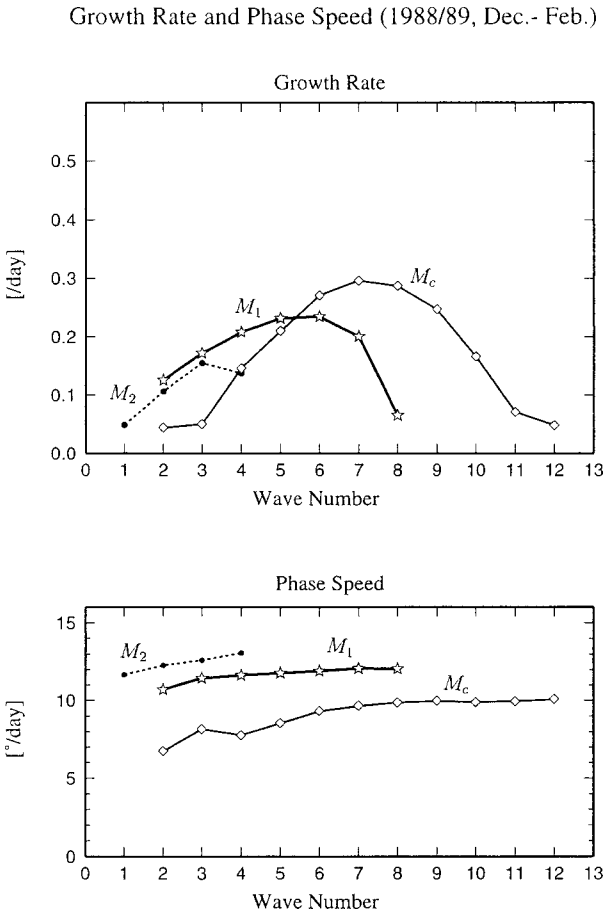

FIG. 9. Growth rates (day^{-1}) and phase speeds (° day^{-1}) of the unstable modes as in Fig. 4 but for the strong polar vortex in 1988/89. The unstable modes are labeled M_C for ordinary Charney modes, M_1 for monopole Charney modes, and M_2 for dipole Charney modes.

of the subtropical jet is 35 m s^{-1} for this winter, which is slightly weaker than the case of 1997/98.

Figure 9 illustrates the growth rates (day^{-1}) and phase speeds (° day^{-1}) of the unstable modes computed for the zonal mean basic state of the strong polar vortex in 1988/89. The most unstable mode at the zonal wavenumber $n = 7$ is identified as the ordinary Charney mode M_C, which appears for $n = 2$ to 12. The Charney mode may be altered to Green mode (Green 1960) for $n = 2$ as documented by Tanaka and Kung (1989). The growth rate of the most unstable mode at $n = 7$ is approximately 0.3 day^{-1} with its *e*-folding time of 3.3 days. It moves eastward with its phase speed of approximately 9° day^{-1} advected by the mean westerly. The most unstable mode M_C is replaced now by the so-called monopole Charney mode M_1 for $n = 2$ to 5 for the strong polar vortex. According to the original work by Tanaka and Kung (1989), the M_1 mode is clearly distinguished from M_2 mode from its monopole structure. It has one amplitude peak in the troposphere as for the ordinary Charney mode and is deep in the sense that the large amplitude extends into the stratosphere for small zonal wavenumbers.

Figure 10 illustrates the meridional-height structures of the geopotential amplitude (in arbitrary unit) and phase (in longitude of ridges) for the monopole Charney modes M_1 at $n = 2$ and 3, M_2 at $n = 1$ and 2, and M_C at $n = 6$ and 7 in Fig. 9. The monopole Charney mode M_1 at $n = 3$ indicates single amplitude maximum at the tropopause level near 60°N. The name of M_1 mode comes from such a structure in comparison with the M_2 mode. The phase tilts westward with respect to height, transporting the eddy heat energy to the north. The structure is similar to M_C mode and is clearly excited by baroclinic instability. The horizontal phase structure shows the eastward phase tilt with respect to latitudes, indicating the poleward eddy momentum flux all the way to the north pole. The meridional-height structure for $n = 2$ exhibits the large amplitude at 10 hPa in addition to the amplitude peak at the tropopause level. Since the structure of the M_1 mode indicates a large meridional extent, the mode has propagated into the stratosphere as expected by Charney and Drazin (1961) for planetary-scale waves. It is not the case for the ordinary Charney modes M_C or dipole Charney modes M_2, which have smaller zonal and meridional scales. The common characteristics to M_1 modes is the poleward eddy momentum flux as inferred from the phase structure. It is important to note that the M_1 mode tends to intensify the polar vortex by those poleward eddy momentum flux. Therefore, the M_1 mode shows a positive feedback with the polar vortex because it appears

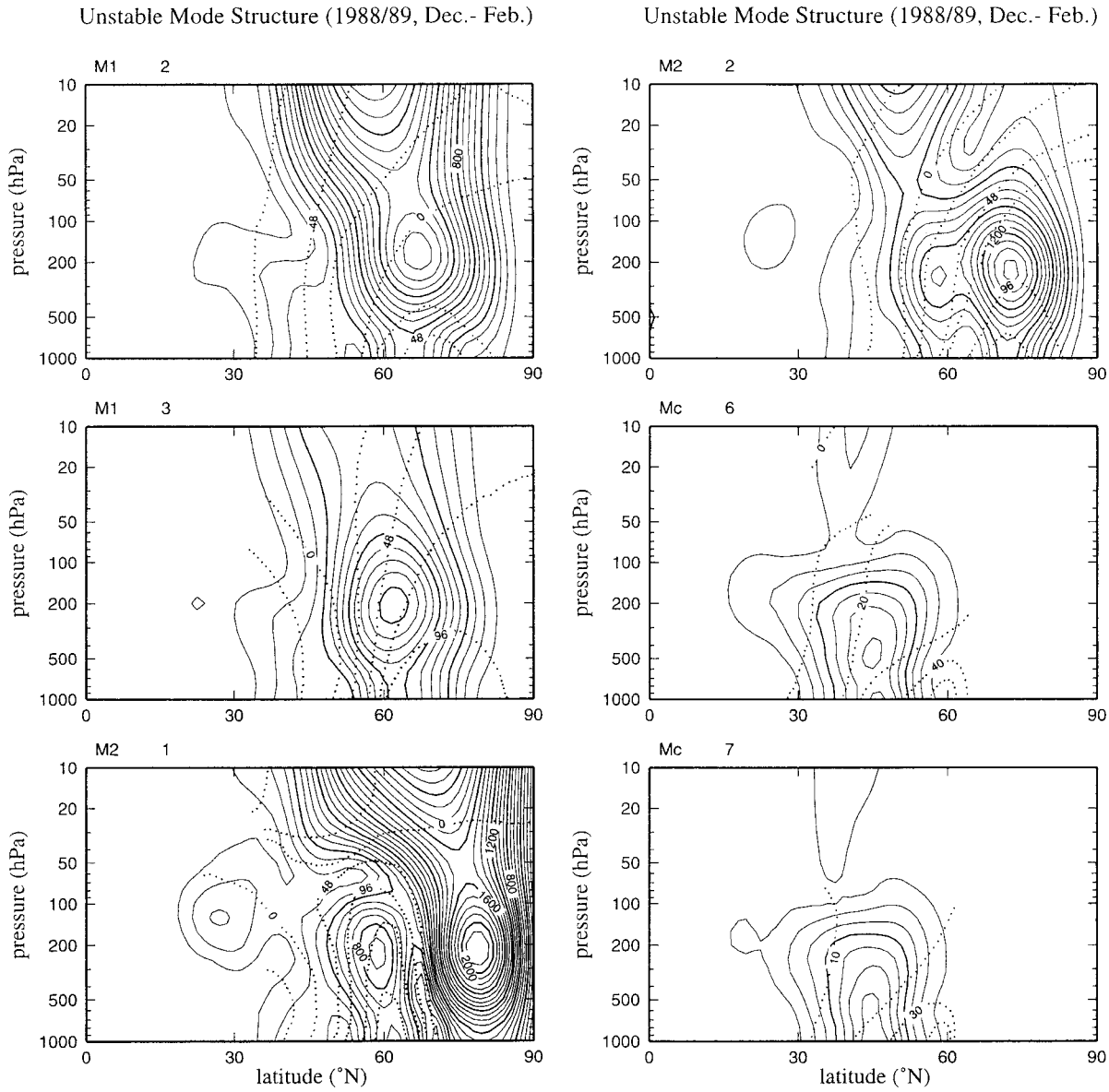

FIG. 10. Meridional-height section of the geopotential amplitude (in arbitrary unit) and phase (in longitude of ridges) for M_1 at zonal wavenumbers $n = 2$ and 3, M_2 at $n = 1$ and 2, and M_C at $n = 6$ and 7 in Fig. 9.

in high latitudes for stronger polar vortex, and it tends to intensify the polar vortex.

b. A case for 1992/93

The winter of 1992/93 is also the year of a typical strong polar vortex as presented in Fig. 11 for the DJF mean. The meridional-height section of zonal mean zonal wind indicates a strong polar night jet over 65°N in the stratosphere. The maximum wind speed in the figure is 40 m s^{-1} at 10-hPa level. The peak line in the wind speed is connected to the subtropical jet at the tropopause level over 30°N. The maximum wind speed of the subtropical jet is 40 m s^{-1} for this winter, which is slightly stronger than the case of 1988/89. The wind distribution is quite similar to that of 1988/89 and is characterized by the strong polar night jet.

Figure 12 illustrates the growth rates (day^{-1}) and phase speeds ($^\circ$ day^{-1}) of the unstable modes analyzed for the strong polar vortex in 1992/93. The most unstable Charney mode M_C appears for $n = 1$ to 12. The growth rate is approximately 0.4 day^{-1} with its e-folding time of 2.5 days at the zonal wavenumber $n = 8$. It moves eastward with its phase speed of approximately 8° day^{-1} advected by the mean westerly.

The most unstable mode is replaced by the M_1 mode for planetary waves of $n = 1$ to 4. The M_1 mode moves eastward with its phase speed of approximately 13° day^{-1}.

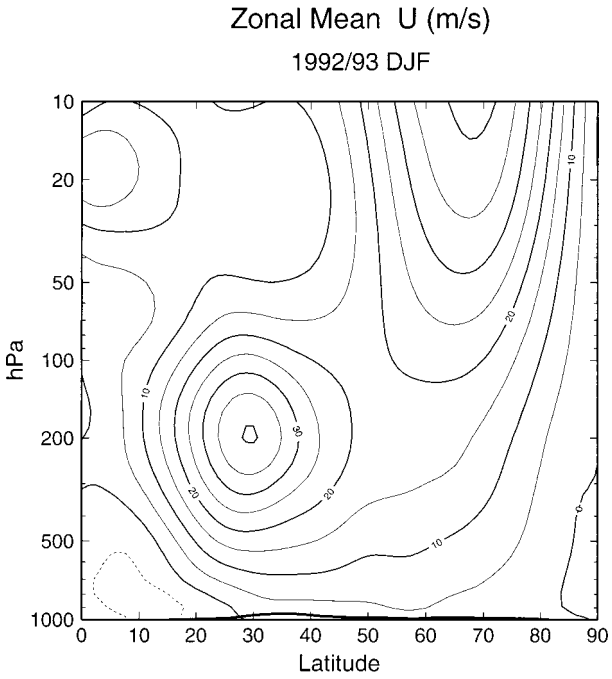

FIG. 11. As in Fig. 8 but for DJF in 1992/93 (another case of the strong polar vortex).

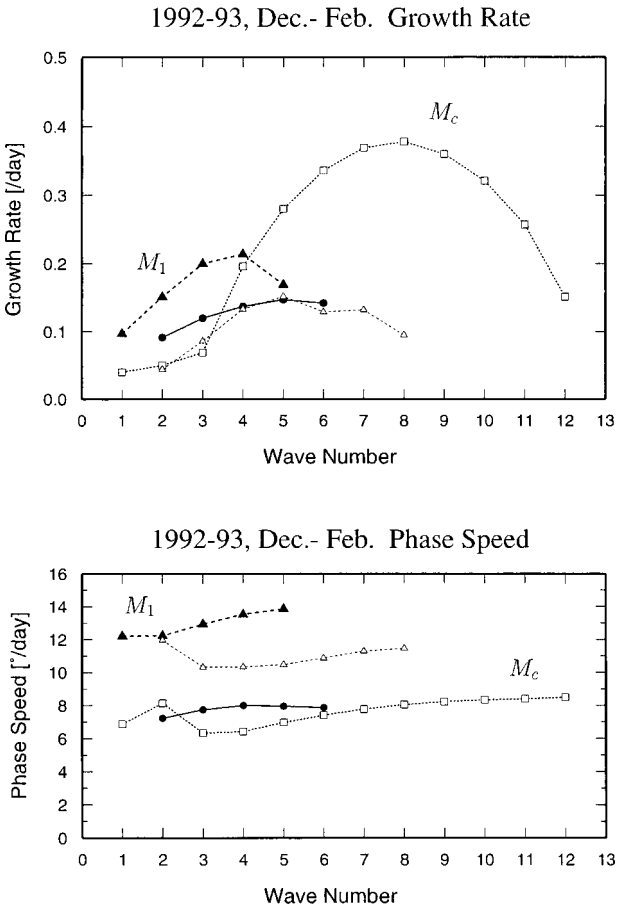

FIG. 12. As in Fig. 9 but for the strong polar vortex of 1992/93 in Fig. 11.

It is important to note that the M_1 mode appears as the dominant mode in planetary waves when the polar jet is strong and is absent when the polar jet is absent. We may infer this from the fact that the M_1 mode would be excited by the baroclinicity associated with the polar jet. The origin of the M_1 mode will be identified in the next experiment.

6. Results for a hypothetical zonal mean zonal wind without the subtropical jet

According to the traditional studies of baroclinic instability (e.g., Green 1960; Garcia and Norscini 1970; Hartmann 1979), we can identify M_2 and M_3 modes as the higher-order meridional modes of the M_C mode that have nodes in the meridional direction. Similarly, the Green mode M_G analyzed by Tanaka and Kung (1989) is identified as the higher-order vertical modes of the M_C mode that have nodes in the vertical direction. Such modes with nodes in the vertical are referred to as Burger modes (Burger 1958; Garcia and Norscini 1970). For a quite general model domain with an open upper boundary over a sphere, as in this study, the baroclinic instabilities may contain those higher-order modes at a time in addition to the principal M_C mode. The M_1 mode, however, was not identified from the viewpoint of the higher-order modes of the M_C mode. It has been an open question to identify the M_1 mode. The M_1 mode shows a similar structure to the M_C mode to large extent, but it appears always in higher latitudes with larger meridional structure.

The answer to this question is resolved somewhat in a different context. Our 3D normal mode expansion method is applied to the Martian atmosphere in Tanaka and Arai (1999) to investigate baroclinic–barotropic instabilities in the Martian atmosphere. The basic state of the zonal mean flow observed by the thermal mapper boarded in the *Viking* spacecraft exhibits a zonal mean zonal wind with a polar jet in high latitudes, but with no subtropical jet in the Martian atmosphere. The dominant unstable mode solved for such a Martian atmosphere appears to be the M_1 mode. Moreover, there is no M_C mode because there is no subtropical jet in the Martian atmosphere. Inspired by this finding, we demonstrate the eigenvalue analysis in this study for such a hypothetical zonal mean wind without the subtropical jet, using the astronomical parameter set for the Earth.

Figure 13 illustrates the hypothetical zonal mean zonal wind constructed with the strong polar vortex in January 1989. The subtropical jet is removed manually from the figure. The polar night jet of 55 m s^{-1} appears at 10 hPa over 65°N. The line of the wind peak moves southward up to 45°N for lower altitudes.

The solution of the unstable modes for such a hy-

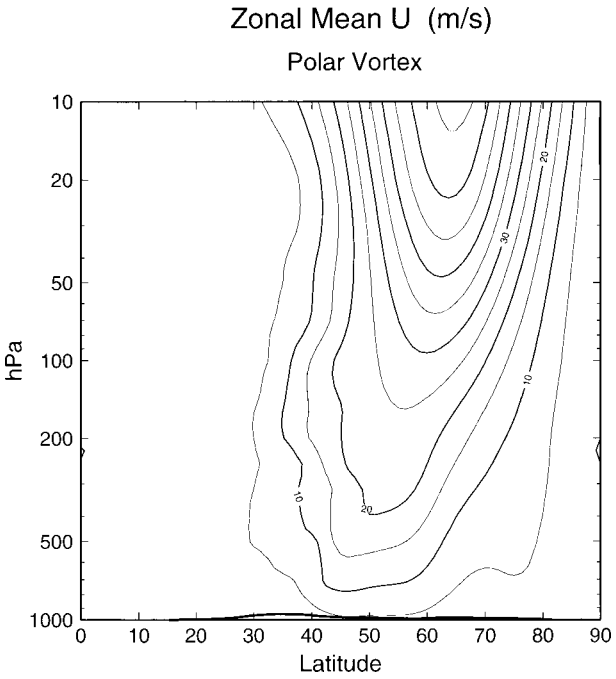

FIG. 13. Meridional-height section of hypothetical zonal mean zonal wind (m s^{-1}) constructed with strong polar vortex in Jan 1989 in the NH. Here, the subtropical jet is removed manually from the basic state.

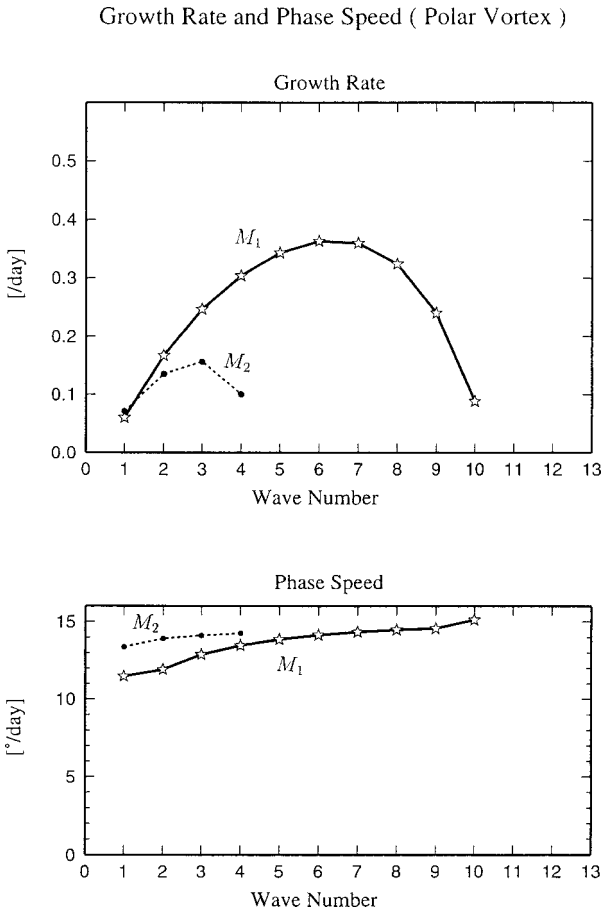

FIG. 14. Growth rates (day^{-1}) and phase speeds (° day^{-1}) of the unstable modes for the hypothetical zonal mean zonal wind in Fig. 13. The unstable modes are labeled M_1 for monopole Charney modes and M_2 for dipole Charney modes.

pothetical basic state is plotted in Fig. 14 as in the same framework with Fig. 12. The most unstable mode appears over $n = 1$ to 10 with its peak growth rate at the zonal wavenumber $n = 6$. The growth rate is approximately 0.4 day^{-1} with its *e*-folding time of 2.5 days. It looks like the ordinary Charney mode M_C in Fig. 12, but actually we find that it is the monopole Charney mode M_1 from its structure. The second unstable mode at $n = 1$ to 4 is identified as M_2 mode. It moves eastward with its phase speed of approximately 13° day^{-1} advected by the mean westerly.

Figure 15 illustrates the meridional-height structures of the geopotential amplitude and phase for the monopole Charney modes M_1 at $n = 2$ and 3. The monopole Charney mode M_1 at $n = 3$ indicates single amplitude maximum at the tropopause level near 60°N. The phase tilts westward with respect to height. It is clearly excited by baroclinic instability associated with the baroclinicity of the polar jet. The horizontal phase structure shows the eastward phase tilt with respect to latitudes, indicating the poleward eddy momentum flux, and the structure is almost identical to that in Fig. 10. The meridional-height structure for $n = 2$ exhibits the large amplitude at 10 hPa in addition to the amplitude peak at the tropopause level. The mode has propagated into the stratosphere. The common fingerprint of the M_1 modes, such as the poleward eddy momentum flux, is identified from the structure.

We are convinced in this study that the M_1 mode is a Charney-type baroclinic instability associated with the baroclinicity of the polar vortex. It may be easily confirmed that the M_C mode becomes an M_1 mode if we continuously move the subtropical jet to the location of the polar jet. Hence, the M_1 mode is dynamically the same Charney mode as M_C but is excited by the baroclinicity of the polar jet in high latitudes. However, when both the subtropical jet and the polar jet exist in the basic state, both the M_C and M_1 modes appear at a time associated with the baroclinicity of the subtropical and polar jets. Once we understand that the M_1 mode is dynamically identical with the M_C mode, we then know that the instability is induced by the negative meridional gradient of basic-state potential vorticity at the thin lower boundary near the surface (Bretherton 1966). It is more sensitive to the mean flow configuration at the lower troposphere rather than the stratospheric polar night jet. We confirmed that the M_1 mode remains strong even if we eliminate the strong polar night jet in the stratosphere as long as the zonal wind shear remains in the troposphere.

It is important to note that the M_1 mode is excited by the baroclinicity associated with the polar vortex, and

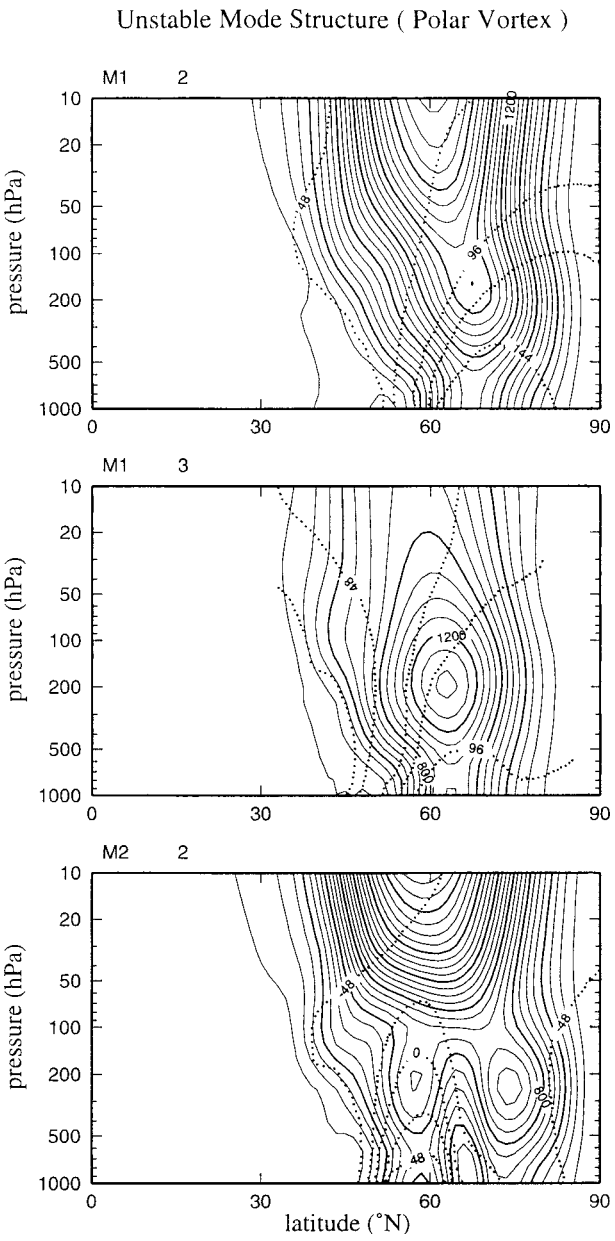

FIG. 15. Meridional-height section of the geopotential amplitude (in arbitrary unit) and phase (in longitude of ridges) for M_1 at zonal wavenumbers $n = 2$ and 3 and M_2 at $n = 2$ in Fig. 14.

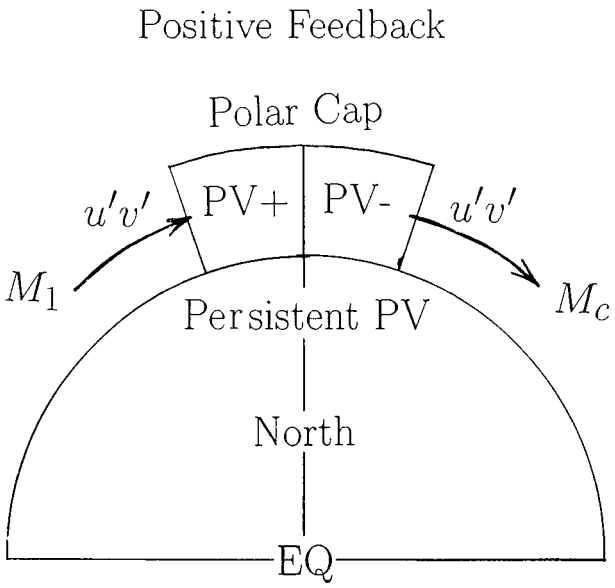

FIG. 16. A schematic diagram of positive feedback between the PV and the monopole Charney mode (M_1) which may cause a persistent polar vortex anomaly. The positive feedback may be detected as AO.

it tends to intensify the polar vortex by its poleward eddy momentum flux. The nature is identical to the M_C mode in midlatitude that is responsible for the zonal index cycle or vacillation phenomenon. The M_1 mode, therefore, should have a positive feedback with the polar vortex because it appears for the stronger polar vortex, and it tends to intensify it.

7. Conclusions and discussion

The Arctic oscillation advocated by Thompson and Wallace (1998) has attracted a lot of attention in recent years. The oscillation is characterized as a seesaw pattern of mass between the arctic region and the surrounding midlatitude ring. The AO is defined by the EOF-1 of the sea level pressure field. The spatial pattern is characterized by its zonally symmetric, annular structure centered at the Arctic and has an equivalent barotropic structure from the surface to the lower stratosphere. It is suggested that the oscillation is induced by the eddy–mean flow interaction, similar to the concept of the index cycle or the vacillation in the SH.

In this study, baroclinic instability of northern winter atmosphere is investigated in the context of the dynamical interpretation of the AO, using a method of 3D normal mode expansion introduced by Tanaka and Kung (1989). The basic states used for the linear stability analysis are the observed zonal mean wind for strong and weak polar vortices. In addition, a hypothetical basic state that has only the polar jet with no subtropical jet is analyzed.

As a result of the eigenvalue problem for such basic states, we obtain a characteristic unstable solution that is dominant in high latitudes when the polar vortex is strong. The mode is called a monopole Charney mode M_1, which transfers eddy momentum from the low latitudes to the polar region. The stronger the polar vortex, the faster the growth of the M_1 mode. On the contrary, the M_1 mode becomes weak or disappears when the polar vortex is weak. We have identified in this study that the M_1 mode is dynamically the same Charney mode as M_C but is excited by the baroclinicity associated with the polar jet in high latitudes.

As is well known in the general circulation study, the Charney mode M_C is excited by the baroclinicity as-

sociated with the subtropical jet and feeds the eddy westerly momentum to the jet. Likewise, the monopole Charney mode M_1 is excited by the baroclinicity associated with the polar jet and tends to feed the eddy westerly momentum to the polar jet. Hence, it is suggested in this study that the M_1 mode should have a positive feedback with the polar vortex, which may in turn result in the occurrence of the annular mode of the Arctic Oscillation.

Figure 16 illustrates a schematic diagram of the positive feedback between the polar vortex PV and the monopole Charney mode M_1. When the polar vortex is strong PV(+), the M_1 mode is excited to feed the westerly momentum to the PV(+). This positive feedback tends to produce strong polar vortex. This dynamics may result in the appearance of the annular mode of AO. The proposed mechanism is analogous to the index cycle in midlatitudes or vacillation in the Southern Hemisphere if it is an oscillatory feedback with certain time lag. The strong PV can be terminated by active M_C since M_C tends to transport the westerly momentum equatorward from the polar vortex. The results of this study are consistent with the diagnostic study by Yamazaki and Shinya (1999), which suggested that the wave–mean flow interaction is constructive at the planetary-scale waves while the synoptic-scale waves contribute destructively to the annual mode. As a future subject, we need to demonstrate the AO using a simple nonlinear model with the parameterized feedback of the M_1 and M_C modes to confirm the proposed scenario in this study.

Acknowledgments. This research was supported by the IARC/FRSGC. The first author appreciates Dr. Takao Sato, Dr. Taroh Matsuno, and Dr. Ryuji Kimura for their meaningful information, suggestions and discussion. The authors appreciate Ms. K. Honda and Mr. M. Hara for their technical assistance.

REFERENCES

Bell, G. D., and M. S. Halpert, 1998: Climate assessment for 1997. *Bull. Amer. Meteor. Soc.,* **79,** S1–S50.

Bretherton, F. P., 1966: Critical layer instability in baroclinic flows. *Quart. J. Roy. Meteor. Soc.,* **92,** 325–334.

Burger, A. P., 1958: Scale consideration of planetary motions of the atmosphere. *Tellus,* **10,** 195–205.

Charney, J. G., 1947: The dynamics of long waves in a baroclinic westerly current. *J. Meteor.,* **4,** 135–162.

——, and P. G. Drazin, 1961: Propagation of planetary-scale disturbances from the lower into the upper atmosphere. *J. Geophys. Res.,* **66,** 83–109.

Exner, F. M., 1925: *Dynamishe Meteorologie*. Springer-Verlag, 415 pp. (Translated by T. Sato, 1998, Iwanami Books, 338 pp in Japanese.)

Garcia, R. V., and R. Norscini, 1970: A contribution to the baroclinic instability problem. *Tellus,* **22,** 239–250.

Green, J. S. A., 1960: A problem in baroclinic stability. *Quart. J. Roy. Meteor. Soc.,* **86,** 237–251.

Hartmann, D. L., 1979: Baroclinic instability of realistic zonal-mean states to planetary waves. *J. Atmos. Sci.,* **36,** 2336–2349.

Kalnay, E. M., and Coauthors, 1996: The NCEP/NCAR 40-Yr Reanalysis Project. *Bull. Amer. Meteor. Soc.,* **77,** 437–471.

Kasahara, A., 1984: The linear response of a stratified global atmosphere to tropical thermal forcing. *J. Atmos. Sci.,* **41,** 2217–2237.

——, and H. L. Tanaka, 1989: Application of vertical normal mode expansion to problems of baroclinic instability. *J. Atmos. Sci.,* **46,** 489–510.

Kitoh, A., H. Koide, K. Kodera, S. Yukimoto, and A. Noda, 1996: Interannual variability in the stratospheric–tropospheric circulation in a coupled ocean–atmosphere GCM. *Geophys. Res. Lett.,* **23,** 543–546.

Kodera, K., M. Chiba, H. Koide, A. Kitoh, and Y. Nikaidou, 1996: Interannual variability of winter stratosphere and troposphere in the northern hemisphere. *J. Meteor. Soc. Japan,* **74,** 365–382.

Namias, J., 1950: The index cycle and its role in the general circulation. *J. Meteor.,* **7,** 130–139.

Proshutinsky, A. Y., and M. A. Johnson, 1997: Two circulation regimes of the wind-driven Arctic Ocean. *J. Geophys. Res.,* **102,** 12 493–12 514.

Shiotani, M., 1990: Low-frequency variations of the zonal mean state of the Southern Hemisphere troposphere. *J. Meteor. Soc. Japan,* **68,** 461–471.

Simmons, A. J., and B. J. Hoskins, 1976: Baroclinic instability on the sphere: Normal modes of the primitive and quasi-geostrophic equations. *J. Atmos. Sci.,* **33,** 1454–1477.

Tanaka, H. L., 1998: Numerical simulation of a life-cycle of atmospheric blocking and the analysis of potential vorticity using a simple barotropic model. *J. Meteor. Soc. Japan,* **76,** 983–1008.

——, and E. C. Kung, 1988: Normal mode energetics of the general circulation during the FGGE year. *J. Atmos. Sci.,* **45,** 3723–3736.

——, and ——, 1989: A study of low-frequency unstable planetary waves in realistic zonal and zonally varying basic states. *Tellus,* **41A,** 179–199.

——, and S. Sun, 1990: A study of baroclinic energy source for large-scale atmospheric normal modes. *J. Atmos. Sci.,* **47,** 2674–2695.

——, and M. Arai, 1999: Linear baroclinic instability in the Martian atmosphere: Primitive equation calculations. *Earth Plan. Space,* **51,** 225–232.

Thompson, D. W. J., and J. M. Wallace, 1998: The arctic oscillation signature in the wintertime geopotential height and temperature fields. *Geophy. Res. Lett.,* **25,** 1297–1300.

Wallace, J. M., and D. S. Gutzler, 1981: Teleconnections in the geopotential height field during the Northern Hemisphere winter. *Mon. Wea. Rev.,* **109,** 784–812.

Walsh, J. E., W. L. Chapman, and T. L. Shy, 1996: Recent decrease of sea level pressure in the central Arctic. *J. Climate,* **9,** 480–486.

Yamazaki, K., and Y. Shinya, 1999: Analysis of the arctic oscillation simulated by AGCM. *J. Meteor. Soc. Japan,* **77,** 1287–1298.